RSC Advances

ROYAL SOCIETY OF CHEMISTRY

www.rsc.org/advances

Journal Name

RSCPublishing

ARTICLE

Template Synthesis of NiO Ultrathin Nanosheets Using Polystyrene Nanospheres and Their Electrochromic Properties

Cite this: DOI: 10.1039/xoxxoooooox

Received ooth January 2012,
Accepted ooth January 2012

DOI: 10.1039/xoxxoooooox

www.rsc.org/

Congcong Zhao[a,b], Cheng Chen[a], Fanglin Du[b], Jinmin Wang[a,]*

Ultrathin nickel oxide（NiO）nanosheets with a thickness of ~10 nm were synthesized by a template method. NiO film was prepared by spin-coating polystyrene@$Ni_2CO_3(OH)_2$ nanostructures on indium tin oxide (ITO) coated glass and calcination process. Electrochromic properties of NiO thin film were investigated in an aqueous alkaline electrolyte (1.0 mol·L^{-1} KOH) by means of transmittance, cyclic voltammetry (CV) measurement. NiO film annealed at 300 °C exhibits noticeable electrochromism with a transmittance modulation of 40.1%, fast coloration and bleaching times of 5.4 and 3.6 s and high coloration efficiency (43.5 $cm^2 \cdot C^{-1}$).

Introduction

Nickel oxide (NiO) has attracted considerable attention due to its broad and potential applications in electrochromic (EC) devices,[1-3] batteries,[4,5] pseudocapacitors,[6] gas sensors[7] and magnetic materials.[8] It has been extensively investigated as an attractive EC material due to its high cyclic stability and high coloration efficiency.[9-11] NiO also exhibits extensive advantages, such as low cost, natural abundance, environmentally friendliness, making it's promising applications in anti-glare mirrors, energy-saving smart windows, and high-contrast displays.[12,13]

The EC properties of materials are closely related to their morphologies and sizes.[14-17] Therefore, researchers have developed various of methods to synthesize NiO nanostructures, including sputtering,[18] chemical bath deposition,[19] sol-gel,[20] electrophoretic deposition,[21] and thermal evaporation.[22] However, it is still difficult to suppress the aggregation of active nanoparticles and increase their surface area, which limits the electrochemical double injection of ions and electrons for high-performance EC devices. A novel and simple fabrication of stable NiO nanostructures with high active surface areas and fast ion and electron diffusion, still needs to be further developed.

Ultrathin nanosheets with one dimension in ultrathin nanoscale (< 10 nm) can obtain a much larger specific surface area, which is benefit for improving the EC performances of materials. Since the discovery of graphene, such two-dimensional ultrathin nanostructures have attracted great attention due to the unique structure and structure-induced promising applications.[23,24] For example, the carbon network grapheme structure with high carrier mobility, mechanical flexibility and chemical stability, could be applied to new electronic materials, novel sensors and storage devices[23,25] Several types of ultrathin nanostructures of transition metal oxides have also been synthesized, including $MnO_2 \cdot 3H_2O$,[26] CeO_2,[27] TiO_2, ZnO, Co_3O_4, WO_3 and Fe_3O_4.[28] However, few literature reports the synthesis of NiO ultrathin nanosheets. Herein, we demonstrate a facile template-synthesis strategy for NiO ultrathin nanosheets by using polystyrene (PS) nanospheres (NSs) as the template. The as-prepared NiO ultrathin nanosheets exhibited excellent EC performances, making them a promising material for high-performance EC devices.

Experimental section

Material preparation

All reagents were purchased from Sinopharm Chemical Reagent Co. Ltd, and used without further purification. PS NSs were used as template which were prepared by micro-emulsion polymerization as described in a previous report.[29] Briefly, $NaHCO_3$ (0.125 g) and sodium dodecylsulfate (0.24 g) were mixed in a beaker with distilled water (160 mL) under stirring at 75 °C for 15 min. Then, styrene monomer (60 mL) was also dispersed in the beaker to form emulsion. Styrene monomer begun to polymerize after adding potassium persulfate (0.40 g) as initiator into the solution. PS colloidal was obtained after

polymerization for 3.5 h. After centrifugation, washing, drying, PS NSs were prepared.

PS NSs (0.30 g), $Ni(NO_3)_2 \cdot 6H_2O$ (0.80 g), and urea (1.20 g) were added into a round bottom flask with distilled water (20 mL) and ethanol (20 mL) under ultrasonic dispersion for 5 min. PS NSs@nanosheets were prepared after heating in oil bath at 90 °C for 8 h. The composite was coated on indium tin oxide (ITO) coated glass by spin-coating. NiO nanosheets film was prepared by calcination at 300 °C for 2 h with a heating rate of 5 °C·min^{-1}.

Characterization

X-ray powder diffraction (XRD) for the phase identification of the product was recorded in the 2θ range from 10 to 80°, using Cu $K\alpha$ (λ = 0.15406 nm) radiation at 40 kV and 40 mA. Transmission electron microscopy (TEM, JEM 2100 F) and scanning electron microscopy (SEM, S-4800) were employed for examining the sample morphologies. Thermogravimetry (TG) was performed between 25 and 500 °C with a heating rate of 2 °C·min^{-1} in air atmosphere. Transmittance spectra for colored and bleached NiO films were in situ measured with a UV-vis spectrophotometer (UV-2550 PC SHIMADZU) in standard cuvettes in the spectral region of 300-800 nm. Bleaching/coloration switching characteristics of the NiO film were recorded with UV-vis spectrophotometer with an absorbance wavelength of 550 nm between -1.0 to 1.4 V. EC properties of the NiO film was performed with 1.0 mol·L^{-1} KOH as the electrolyte, a platinum sheet as the counter electrode and Hg/HgO as reference electrode using a CHI660D electrochemical workstation.

Results and Discussion

Structure and morphology

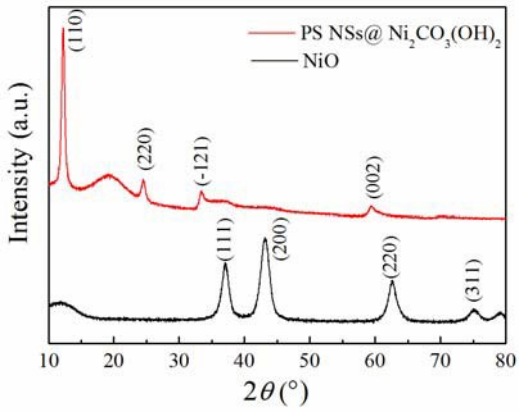

Fig. 1. XRD patterns of PS NSs@$Ni_2CO_3(OH)_2$ composite and NiO nanosheets.

Fig. 1 shows the powder XRD patterns of the as-prepared PS NSs@$Ni_2CO_3(OH)_2$ composite and NiO nanosheets. The XRD pattern of PS NSs@$Ni_2CO_3(OH)_2$ composite are composed of sharp peaks of $Ni_2CO_3(OH)_2$ (JCPDS No. 35-0501) and featureless peak of PS NSs, which is consistent with the XRD patterns shown in Fig. S1 (see Supplementary Information). The XRD pattern of PS NSs is featureless, indicating its amorphous nature. The diffraction peaks of product obtained without PS template while keeping other conditions unchanged can be indexed to monoclinic $Ni_2CO_3(OH)_2$ (JCPDS No. 35-0501). The reaction between Ni^{2+} ions and OH^-, CO_3^{2-} ions formed from the hydrolysis of urea leads to the formation of $Ni_2CO_3(OH)_2$. The XRD pattern of PS NSs@$Ni_2CO_3(OH)_2$ composite is composed of sharp peaks of $Ni_2CO_3(OH)_2$ (JCPDS No. 35-0501) and featureless peak of PS NSs. The diffraction pattern of the product prepared after calcination at 300 °C for 2 h can be ascribed to cubic phase of NiO (JCPDS No. 47-1049).

The thermal behavior of the as-prepared PS NSs@$Ni_2CO_3(OH)_2$ composite and $Ni_2CO_3(OH)_2$ were studied by TG, as shown in Fig. S2 (Supplementary Information). The TG curve shows the main weight loss (21.5%) of $Ni_2CO_3(OH)_2$ is in the temperature range of 285-305 °C, suggesting the decomposition of $Ni_2CO_3(OH)_2$ to NiO. The TG curve of the as-prepared PS NSs@$Ni_2CO_3(OH)_2$ shows a sharp weight loss (~70.5%) from 270 to 320 °C, which is attributed to the decomposition of $Ni_2CO_3(OH)_2$ and the removal of PS.[30] After being calcined at 300 °C for 2 h in air, the PS NSs were removed and $Ni_2CO_3(OH)_2$ is converted to NiO.

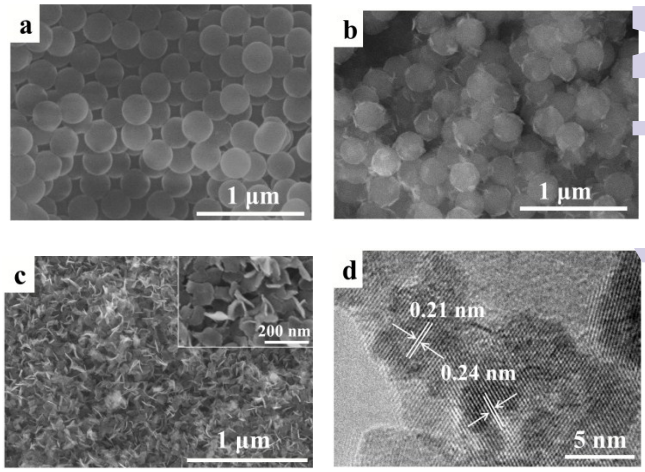

Fig. 2. FESEM images of (a) PS NSs, (b) PS NSs@$Ni_2CO_3(OH)_2$ composite, (c) NiO nanosheets and (d) HRTEM image of NiO nanosheets.

Fig. 2 shows the morphologies of several representative samples. From Fig. 2a, it can be clearly seen that the PS NSs template has a uniform size of ~250 nm and a smooth surface. Fig. 2b suggests that only nanosheets are formed on part of the PS templates surface. Fig. 2c shows the morphology of NiO ultrathin nanosheets films achieved by calcination of the spin coated PS NSs@$Ni_2CO_3(OH)_2$ composite film. NiO nanosheets are formed with ~10 nm in thickness, thinner than NiO nanosheets (~200nm) fabricated by hydrothermal method without using PS.[31] In order to study the effect of PS NSs template and urea concentration on the morphology, experiments are conducted in the absence of the PS NSs templates and doubled urea content while keeping other conditions unaltered (see Fig. S3, Supplementary Information). HRTEM image of NiO ultrathin nanosheets is also shown in Fig. 2. Clear lattice fringes can be seen in Fig. 2d, indicating a good crystallinity of the as-synthesized cubic phase of NiO ultrathin nanosheets. The HRTEM image shows the lattice fringes with the d-spacings of 0.24 and 0.21 nm, corresponding to the (111) and (200) planes of cubic NiO, respectively.

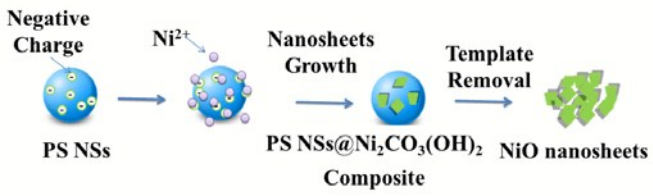

Fig. 3. Schematic formation mechanism of NiO nanosheets.

Fig. 3 illustrates the mechanism for synthesizing NiO nanosheets. It is well known that there are negatively charged groups on the surface of PS NSs which could attract Ni^{2+} ions in $Ni(NO_3)_2$ solution through adsorption.[32] $[Ni(NH_3)_6]^{2+}$ coordination compound is formed by the reaction of Ni^{2+} ions and NH_3, which is in accordance with the previous report.[33] When NH_3 was released by urea and reaction (3), (4), (5) take place, reaction (2) will shift to the left-hand side in order to keep reaction (5) going continuously. With continuing of reaction, the $Ni_2CO_3(OH)_2$ nanoclusters were obtained. NH_3 molecules can be adsorbed onto (002) crystal plane of $Ni_2CO_3(OH)_2$ crystal nucleus, reducing the growth rate of *c*-axis as proved in previous report.[34] As a result, ultrathin nanosheets growing along the two-dimensional plane perpendicular to *c*-axis were formed. After calcination of PS NSs@$Ni_2CO_3(OH)_2$ composite spheres in air, PS NSs are removed and NiO nanosheets were obtained.

$$CO(NH_2)_2 + H_2O = CO_2 + 2NH_3 \quad (1)$$
$$Ni^{2+} + 6NH_3 \leftrightarrow [Ni(NH_3)_6]^{2+} \quad (2)$$
$$CO_2 + H_2O \leftrightarrow 2H^+ + CO_3^{2-} \quad (3)$$
$$NH_3 + H_2O \leftrightarrow NH^{4+} + OH^- \quad (4)$$
$$2Ni^{2+} + 2OH^- + CO_3^{2-} = Ni_2CO_3(OH)_2 \quad (5)$$

EC Properties

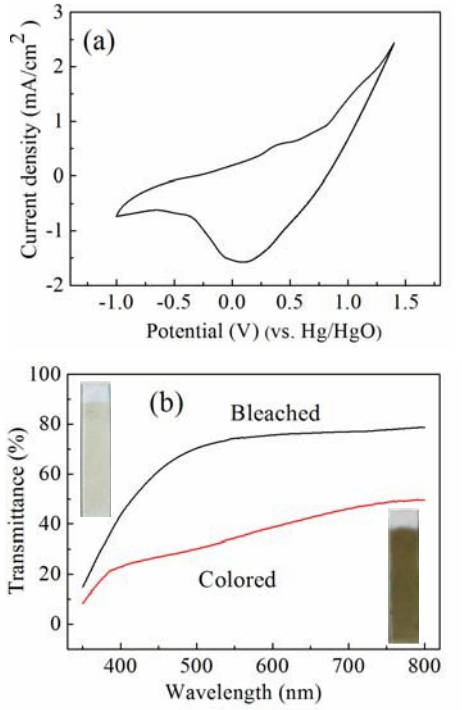

Fig. 4. (a) CV curve of NiO nanosheets film, (b) color changes and transmittance spectra of the as-prepared EC film measured at colored and bleached states.

The cyclic voltammetry (CV) measurement of NiO nanosheets film recorded between -1.0 to 1.4 V with a scan rate of 0.1 $V \cdot s^{-1}$ are shown in Fig. 4a. The intercalation of OH^- ions accompanies oxidation of Ni^{2+} to Ni^{3+} ions, resulting in a brow color. The deintercalation of OH^- ions and reduction of Ni^{3+} to Ni^{2+} ions leads to transparent color of NiO film. The recorded current results from OH^- ions intercalation/deintercalation and electron transfer between Ni^{2+} ions and Ni^{3+} ions, which can be attributed to the following electrochemical reactions.[35]

NiO (transparent) + z (OH^-) ↔ NiOOH (brown) + z e^- (6)

Fig. 4b shows the in situ transmittance spectra of the NiO nanosheets film recorded at -1.0 and 1.4 V, in the wavelength range from 350 to 800 nm. It can be seen that the as-prepared ultrathin NiO nanosheets film is almost colorless, at bleached state. When applying a voltage of 1.4 V, the NiO film displayed a brown color. The transmittance peak shows that the corresponding maximum absorbance wavelengths should be in the range of 500-600 nm. Here, a wavelength of 550 nm used in many literatures reported for NiO films[31] was selected as the maximum absorbance wavelength of the as-prepared ultrathin NiO nanosheets film. The transmittance variation betwe... colored and bleached states was 40.1% at 550 nm. The high transmittance modulation suggests that NiO film possesses good contrast because of ultrathin nanosheets nature, large surface area and increased textural boundaries. This ultrath... structure can increase the effective surface area that could accelerate OH^- ions intercalation/deintercalation and electron transfer between the electrode and electrolyte.

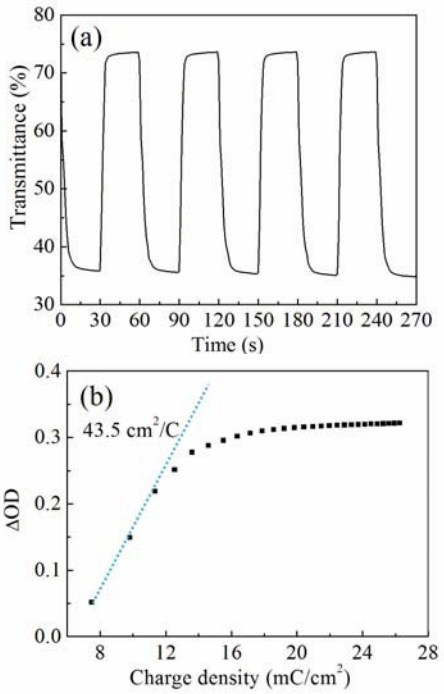

Fig. 5. (a) Switching time characteristics between the bleached and colored states at 550 nm, (b) optical density variation with respect to the charge density recorded at 550 nm.

The switching time between the bleached and colored states is a very important factor in practical applications of EC systems. The switching time characteristics of the NiO fil... were measured. Obvious color changes can be observed durin... the switching. The coloration and bleaching times ar...

calculated as the time required for 90% changes in the whole transmittance modulation at 550 nm. The coloration time and bleaching time of 90% changes ($t_{c(90\%)}$, $t_{b(90\%)}$) were found to be 5.4 and 3.6 s. Compared with NiO nanoplate film fabricated by the hydrothermal method ($t_{c(90\%)}$ = 26.4 s and $t_{b(90\%)}$ = 44 s),[32] the coloration and bleaching time for 90% modulation is shorter, which indicates the ultrathin nanosheets with large surface area could facilitate the ions intercalation/deintercalation by reducing their diffusion path lengths. Coloration efficiency (CE), defined as the change in the optical density ($\Delta OD = \log(T_{bleach}/T_{color})$) per unit charge density (Q/A), and can be calculated according to the formula: $CE = \Delta OD/(Q/A)$. Fig. 5b shows the in situ ΔOD plots recorded at λ=550 nm versus the ejected electronic charge density (Q). The CE was extracted as the slope of the line fitted to the linear region of the curve. The CE of the NiO nanosheets film is calculated to be 43.5 $cm^2 \cdot C^{-1}$. In comparison with CE values of EC films also used PS NSs as template, it is found that the CE of the as-prepared NiO nanosheets film is higher than those of ordered porous NiO film (41 $cm^2 \cdot C^{-1}$),[36] and Co_3O_4 ordered bowl-like array film (29 $cm^2 \cdot C^{-1}$).[37]

Conclusions

In summary, NiO ultrathin nanosheets with a thickness of ~10 nm were synthesized by using PS NSs as the template. NiO EC films have been successfully prepared by spin-coating and calcination process. NiO flim annealed at 300 °C exhibits good EC behavior with transmittance modulation of 40.1%, fast coloration and bleaching times of 5.4 and 3.6 s and high coloration efficiency (43.5 $cm^2 \cdot C^{-1}$), showing a promising application in high-performance energy-saving EC smart windows.

Acknowledgements

We would like to thank support from The Program for Professor of Special Appointment (Eastern Scholar) at Shanghai Institutions of Higher Learning (No. 2013-70), Shanghai Pujiang Program (No. 13PJ1403300), “Shu Guang” project supported by Shanghai Municipal Education Commission and Shanghai Education Development Foundation (No. 13SG55), Innovation Program of Shanghai Municipal Education Commission (No. 13ZZ138), National Natural Science Foundation of China (NSFC) (No. 61376009, No. 51272115), the Natural Science Foundation of Shandong Province (No. ZR2012EMM001), the Opening Project of State Key Laboratory of High Performance Ceramics and Superfine Microstructure (SKL201313SIC), and the Opening Project of State Key Laboratory for Modification of Chemical Fibers and Polymer Materials, Donghua University (LK1221).

Notes and references

[a] School of Environmental and Materials Engineering, College of Engineering, Shanghai Second Polytechnic University, Shanghai 201209, China.
E-mail: wangjinmin@sspu.edu.cn, Tel: +86-21 50217725, Fax: +86-21 50217725.
[b] School of Materials Science and Engineering, Qingdao University of Science and Technology, Qingdao 266042, China.

1 M. Mihelčič, A. Š. Vuk, I. Jerman, B. Orel, F. Švegl, H. Moulki, C. Faure, G. Campet and A. Rougier, *Sol. Energy Mater. Sol. Cells,* 2014, **120**, 116-130.
2 H. Moulki, C. Faure, M. Mihelčičb, A. Šurca Vuk, F. Šveglc, B. Orel, G. Campet, M. Alfredsson, A. V. Chadwick, D. Gianolio and A. Rougier, *Thin Solid Films*, 2014, **553**, 63-66.
3 X. H. Xia, J. P. Tu, J. Zhang, X. L. Wang, W. K. Zhang and H. Huang, *Electrochim. Acta*, 2008, **53**, 5721-5724.
4 T. R. Sanchis, A. Guerrero, E. Azaceta, R. T. Zaera and G. G. Belmonte, *Sol. Energy Mater. Sol. Cells*, 2013, **117**, 564-568.
5 J. M. Ma, J. Q. Yang, L. F. Jiao, Y. H. Mao, T. H. Wang, X. C. Duan, J. B. Lian and W. J. Zheng, *CrystEngComm.*, 2012, **14**, 453-459.
6 X. H. Xia, J. P. Tu, X. L. Wang, C. D. Gu and, X. B. Zhao, *J. Mater. Chem.*, 2011, **21**, 671-679.
7 C. Li, C. H. Feng, F. D. Qu, J. Liu, L.H. Zhu, Y. Lin, Y. Wang, F. Li, J. R. Zhou and S. P. Ruan, *Sensor Actua.t B*, 2015, **207**, 90-96
8 S. Chatterjee, A. Bera, A. J. Pal, *ACS Appl. Mater. Interfaces*, 2014, **6**, 20479-20486
9 K. K. Purushothaman, G. Muralidharan, *J. Sol–Gel Sci.Technol.*, 2008, **46**, 190-194.
10 M. Chigane, M. Ishikawa, *Electrochim. Acta*, 1997, **42**, 1515-1519.
11 E. Avendano, L. Berggren, G. A. Niklasson and C. G. Granqvist, *Thin Solid Films*, 2006, **496**, 30-36.
12 C. G. Granqvist, *Adv. Mater.*, 2003, **15**, 1789-1803.
13 D. Y. Ma, G. Y. Shi, H. ZH. Wang, Q. H. Zhang and Y. G. Li, *J. Mater. Chem. A*, 2014, **2**, 13541-13549
14 H. Ling, J. L. Lu, S. -L. Phua, H. Liu, L. Liu, Y. Z. Huang, D. Mandler, P. S. Lee and X. H. Lu, *J. Mater. Chem. A*, 2014, **2**, 2708-2717
15 Q. L. Jiang, F. Q. Liu, T. Li and T. Xu, *J. Mater. Chem. C,* 2014, **2**, 618-621.
16 R. A. Patil, R. S. Devan, J.-H. Lin, Y.-R. Ma, P. S. Patil, Y. Liou, *Sol. Energy Mater. Sol. Cells*, 2013, **112**, 91- 96.
17 H. W. Zhang, G. T. Duan, G. Q. Liu, Y. Li, X. X. Xu, ZH. F. Dai, J. J. Wang and W. P. Cai, *Nanoscale*, 2013, **5**, 2460-2468.
18 E. Avendano, A. Azens, J. Isidorsson, R. Karmhag, G. A. Niklasson and C. G. Granqvist, *Solid State Ionics*, 2003, **165**, 169-173.
19 X. H. Xia, J. P. Tu, J. Zhang, X. L. Wang, W. K. Zhang and H. Huang, *Sol. Energy Mater. Sol. Cells*, 2008, **92**, 628-633.
20 Y. N. Liu, C. Y. Jia, Z. Q. Wan, X. L. Weng, J. L. Xie and L. J. Deng, *Sol. Energy Mater. Sol. Cells*, 2015, **132**, 467-475.
21 M. Hakamada, A. Moriguchi and M. Mabuchi, *J. Power Sources*, 2014, **245**, 324-330.
22 S. Pereira, A. Goncalves, N. J. Correia, L. Pinto, R. Pereira, Martins and E. Fortunato, *Sol. Energy Mater. Sol. Cells*, 2014, **120**, 109-115.
23 K. S. Novoselov, A. K. Geim, S. V. Morozov, D. Jiang, Y. Zhang, S. V. Dubonos, I. V. Grigorieva and A. A. Firsov, *Science* 2004, **306**, 666-669
24 M. J. Allen, V. C. Tung and R. B. Kaner, *Chem. Rev.*, 2010, **110**, 132-145.
25 A. K. Geim, K. S. Novoselov, *Nat. Mater.*, 2007, **6**, 183-191.
26 J. M. Wang, E. Khoo, J. Ma and P. S. Lee, *Chem. Commun.*, 2010, **46**, 2468-2470.
27 T. Yu, J. Joo, Y. I. Park and T. Hyeon, *J. Am. Chem. Soc.*, 2006, **128**, 1786-1787.
28 Z. Q. Sun, T. Liao, Y. H. Dou, S.-M. Hwang, M.-S. Park, L. Jiang, J. H. Kim and S. X. Dou, *Nat. Commun.*, 2014, **5**, 3813-3822.
29 C. E. Reese, C. D. Guerrero, J. M. Weissman, K. Lee, S. A. Asher, *J.*

Colloid Interf. Sci., 2000, **232**, 76-80.
30 S. J. Ding, T. Zhu, J. S. Chen, Z. Y. Wang, C. L. Yuan and X. W. Lou, *J. Mater. Chem.*, 2011, **21**, 6602-6606.
31 D. Y. Ma, G. Y. Shi, H. Z. Wang, Q. H. Zhang and Y. G. Li, *Nanoscale*, 2013, **5**, 4808-4815
32 Z. Z. Gu, H. H. Chen, S. Zhang, L. G. Sun, Z. Y. Xie, Y. Y. Ge, *Colloid Surf. A-Physicochem. Eng. Asp.*, 2007, **302**, 312-319.
33 Y. Li, B. Tan and Y. Wu, *Chem. Mater.*, 2008, **20**, 567-576.
34 G. H. Li, X. W. Wang, H. Y. Ding and T. Zhang, *RSC Adv.*, 2012, **2**, 13018-13023.
35 L. D. Kadam and P. S. Patil, *Sol. Energy Mater. Sol. Cells*, 2001, **69**, 361-369.
36 Y. F. Yuan, X. H. Xia, J. B. Wu, Y. B. Chen, J. L. Yang and S. Y. Guo, *Electrochim. Acta*, 2011, **56**, 1208-1212.
37 X. H. Xia, J. P. Tu, J. Zhang, J. Y. Xiang, X. L. Wang and X. B. Zhao, *ACS Appl. Mater. Inter.,* 2010, **2**,186-192.